Microbiology, Metabolites and Biotechnology
MMB
The former ARMMT
Iranian Research Organization for Science and Technology

# Improvement of biochemical properties of asparaginase by immobilization on cysteine functionalized magnetic Fe3O4@Au NPs

**Ali Reza Montazeri[1], Parvaneh Maghami[1], Hedayatollah Ghourchin[2], Hamid Moghimi[3*]**

[1]*Department of Biology, Science and Research Branch, Islamic Azad University, Tehran, Iran*
[2]*Laboratory of Bioanalysis, Institute of Biochemistry and Biophysics, University of Tehran, Tehran, Iran.*
[3]*Department of Microbial Biotechnology, School of Biology, College of Science, University of Tehran, Tehran, Iran*

**Article Info**

**Document Type:**
Research Paper

**Received** 14/01/2023
**Received in revised form** 15/02/2023
**Accepted** 16/02/2023

**Keywords:**
Asparaginase;
Immobilization;
Core-shell;
Iron-gold nano-particles

**Abstract**

L-Asparaginase converts L-asparagine to L-aspartic acid and causes cancer cells to starve. The main idea of the current study was to improve the biochemical properties of this enzyme using immobilization onto modified magnetic nano-particles (NPs). To this end, $Fe_3O_4$ NPs were synthesized, coated with an Au shell, and conjugated with cysteine. The formation of NPs and core-shell structures and their morphology were confirmed using Fourier Transform Infrared spectroscopy (FTIR), Energy Dispersive X-Ray (EDX), VU-Vis, Scanning Electron Microscopy (SEM), and Transmission Electron Microscopy (TEM). Also, Circular Dichroism (CD) and fluorescence spectroscopy were employed for the analysis of the secondary and tertiary structures of the immobilized L-ASNase. The alterations in kinetic parameters of the immobilized enzyme were analyzed using a Lineweaver-Burk plot. The results of instrumental chemistry analysis confirmed the formation of NPs and core-shell structure, and cysteine binding with the core-shell. Based on CD and fluorescence results, no significant changes were observed in the secondary and tertiary structures of the immobilized enzyme compared to the free one. Kinetic parameters of the immobilized enzyme improved compared to the free enzyme so that Km decreased from 4.43±0.05 to 3.75±0.12 mM and Vmax increased from 187.23±11 to 224.78±16 μM min-1mg-1. Also, the stability of the immobilized enzyme improved with acidic and alkaline pH values compared to the free one at temperatures higher than 50 $^0$C. In addition, the reusability of the immobilized enzyme was superior to the free enzyme, with the immobilized enzyme maintaining 72% of its activity after 15 cycles of catalytic reaction. The immobilized enzyme showed an 86% residual activity after 120 min incubation with trypsin, which was higher than the free enzyme (37%). According to the results of this study, immobilization of L-ASNase onto magnetic NPs can be an efficient strategy to enhance the biochemical properties of this enzyme.

## 1. Introduction

L-Asparaginase (L-ASNase) is a well-characterized enzyme that is considered a potent antineoplastic agent. L-ASNase catalyzes L-asparagine to L-aspartate and creates L-asparagine deficiency in cancerous cells. Given the fact that cancer cells are unable to synthesize this amino acid, they lose their ability for uncontrolled growth (Batool et al., 2016). The

*Corresponding author. Tel: *+982166415495*
E-mail address: hmoghimi@ut.ac.ir
DOI: 10.22104/MMB.2023.6061.1086

production of L-ASNase has been reported in various types of plant, fungal, and bacterial species. For example, L-ASNase isolated from Escherichia coli and Erwinia chrysanthemi is produced on a large scale and applied to treat lymphoblastic leukemia (Narayana et al., 2008). The improvement of biological activity and stability of this therapeutic enzyme has been interesting to researchers. For instance, conjugation of L-ASNase with polyethylene glycol (PEG) increased its resistance against high temperatures (65 $^0$C) and made it more active (Soares et al., 2002). In addition, the conjugation of L-ASNase with aluminum oxide and titanium oxide NPs increased the cytotoxic activity of L-ASNase on MOLT-4 tumor cells and its affinity to L-asparagine. Also, the shelf life of the conjugated enzyme was increased compared to the free one (Agrawal & Kango, 2019).

Enzyme immobilization is a key technique in biotechnology that improves the physicochemical properties of enzymes and makes them suitable for applications in industries. The main idea of this technology is to increase the enzymes' catalytic activity, their affinity to the substrate, and their physical stability against environmental conditions (Federsel et al., 2021). For example, studies have shown that the immobilization of α-amylase on $Fe_3O_4$ NPs increased thermal stability, an affinity for the substrate, and reusability of this enzyme so that at the end of 6 cycles of reaction, the enzyme sustained 85% of its native activity (Sohrabi et al., 2014). In another study, the effect of the immobilization process on the stability and activity of lipase was evaluated (Dong et al., 2012). The results of this study suggested that the stability of the immobilized enzyme against thermal and inactivation increased, and it retained 82.5% of its activity after 6 cycles of reaction. Cross-linking, ionic and electrostatic bonding, and encapsulation are methods that are applied to immobilize enzymes on various matrices like biological polymers (e.g., chitosan, alginate, starch, and cellulose), mineral materials (e.g., zeolites, ceramics, silica, and activated carbon) and NPs (e.g., $Fe_3O_4$) (Bilal et al., 2018; Datta et al., 2013; Lee et al., 2020). Core-shell nano-materials have attracted interest due to their bifunctional nature. Excellent magnetic sensitivity and biocompatibility are the most important characteristics of metal-based magnetic core-shell NPs (León Félix et al., 2017). The remarkable optical properties of a $Fe_3O_4$@Au core-shell make it suitable for biomedical applications (e.g., imaging and photothermal therapy). However, the solubility of a $Fe_3O_4$@Au core-shell in water is relatively low. Hydrophilic thiols can solve this problem (Salihov et al., 2015). Core-shell NPs are mostly cleared from the body through the liver, spleen, and kidneys which prevents their access to target sites. This process is controlled by the core-shell NPs' physicochemical properties of (e.g., charge, size, and shape) (Tamer et al., 2010).

Fe3O4 NPs show high guidability and adaptability in different conditions. On the other hand, normal cell toxicity was observed while using these NPs as drug carriers. Due to its highly neutral and biocompatible nature, covering these NPs with a gold shell resolves this problem to a great extent. Cysteine is a thiol organic cross-linker that readily binds to gold. The short length of carbon chains is expected to result in L-ASNase strongly binding to NPs surface, which improves the enzyme's biochemical characteristics. The major aim of the current study was first to immobilize L-ASNase onto the $Fe_3O_4$@Au core-shell and then to examine its effects on the physicochemical stability of the enzyme.

## 2. Materials and Methods

The *Escherichia coli* L-ASNase with 10000 IU was from Leunase®. All analytical grade chemicals were obtained from the Merck Co.

### 2.1 Fe3O4 NPs synthesis

Synthesis of $Fe_3O_4$ NPs was performed according to the co-precipitation reaction. To this aim, 0.4 g of $FeCl_3$ and 0.6 g of $FeCl_2$ were added into 80 ml of ultra-pure water, $N_2$ gas was added, and the prepared solution was stirred at 50 $^0$C for 30 min. Then, 5 ml of NaOH (2 M) was added, and after the formation of dark color sediments,

the temperature was increased to 70 $^0$C and stirred for 4 h under alkaline conditions (pH 12). Finally, the solution was allowed to cool to ambient temperature, and the sediments were collected with a magnet (Hariani et al., 2013).

### 2.2 $Fe_3O_4$@Au core-shell NPs synthesis

To synthesize the iron-gold core-shell, the synthesized $Fe_3O_4$ NPs were added to ultra-pure water, and the temperature was increased up to the boiling point. Then, 15 mM of chloroauric acid was subjoined, and the solution was stirred for 10 min. After adding $Na_3C_6H_5O_7$, the solution was allowed to boil until the burgundy color appeared. Finally, the mixture was stirred for 10 min and cooled to room temperature (Yazdani & Seddigh, 2016).

### 2.3 Cysteine functionalization of $Fe_3O_4$@Au core-shell NPs

Initially, 50 mg of $Fe_3O_4$@Au NPs was sonicated for 5 min. Then, 100 µl of cysteine solution ($5 \times 10^{-4}$ M) was added into phosphate buffer (pH 6.8) containing NPs as a cross-linker, and the solution was kept for 24 h at 4 $^0$C.

### 2.4 Characterization of NPs

The crystalline structures of $Fe_3O_4$ and $Fe_3O_4$@Au NPs were assessed using XRD, and the crystal structures were taken with Cu-Lα radiation for the 2θ range of $2^0$ to $80^0$. In addition, Au binding onto $Fe_3O_4$ NPs and the elemental composition of NPs were analyzed using Energy Dispersive X-Ray Spectroscopy methods (EDX) (Ronteck Xflash detector analyzer), respectively. Analysis of NPs morphology and size was done by Scanning Electron Microscopy (SEM) and Transition Electron Microscopy (TEM), respectively. FTIR with KBr disks were used to investigate the functional groups on the surface of the NPs after modification and combination with L-ASNase. FTIR spectra were recorded in the range 500 - 3000 $cm^{-1}$.

### 2.5 Conjugation of the enzyme with $Fe_3O_4$@Au@cysteine

Firstly, the modified NPs were dissolved in 20 ml of ultra-pure water and 4 µl of 1-Ethyl-3-(3-dimethyl amino propyl) carbodiimide EDC (800 µg/ml) and 4 µl of N-Hydroxysuccinimide (NHS) (640 µg/ml) were added into this solution and stirred for 1 h. Next, the enzyme was gently added to the solution and incubated at 4 $^0$C for 4 h. Finally, NPs containing L-ASNase were collected with a magnet and kept at 5 $^0$C.

### 2.6 Determination of enzyme catalytic activity

A method based on ammonia production was employed to measure the catalytic activity of L-ASNase. Briefly, 0.2 ml (50 µg) of free and immobilized enzyme was stirred with 2.75 ml (10 mM) of L-asparagine and 1 M phosphate buffer (pH 7.3). The prepared solution was incubated at 37 $^0$C for 30 min. The hydrolysis reaction of L-ASNase was stopped by adding 2 M trichloroacetic acid (TCA). Next, immobilized L-ASNase was collected from the solution with a magnet. Then, the reaction solution was mixed with 0.5 ml of Nessler reagent and 5 ml of ultra-pure water. Finally, catalytic activity was measured by spectrophotometry at 430 nm (Wriston & Yellin, 1973).

### 2.7 Enzyme conjugation efficiency

Conjugation efficiency was calculated using equation 1. Where $E_0$ is the total enzyme concentration and $E_1$ is the enzyme concentration in the washing solution. The concentration of the enzyme was calculated using the Bradford method.

$$\text{Conjugation efficiency} = \left[\frac{E0-E1}{E0}\right] \times 100 \qquad (1)$$

### 2.8 Biochemical properties of free and immobilized enzyme

#### 2.8.1 Optimum temperature and pH

Several temperatures (25-75 $^0$C) and pH values (4-12) were prepared to examine the relative activity of free and immobilized L-ASNase.

### 2.8.2 Free and immobilized enzyme kinetic analysis

To this aim, the velocity of the catalytic reaction was determined by preparing several levels of L-asparagine. Then, the reciprocal of velocity (1/v) and substrate concentration (1/s) were calculated, and the Lineweaver Burk plot (Michalis–Menten linear plot) was drawn. Finally, Km and Vmax were calculated as follows:

$$\frac{1}{v} = \left(\frac{Km}{Vmax} \times \frac{1}{s}\right) + \frac{1}{Vmax} \quad (2)$$

### 2.9 Far-ultraviolet CD study of the enzyme

Free and conjugated enzyme secondary structures were analyzed using Circular Dichroism at (190-260 nm). The reports of the CD were processed by the CDNN 2.1 algorithm. All spectra were collected by subtracting sample spectra from buffer one.

### 2.10 Enzymes fluorescence spectroscopy

Enzymes fluorescence analysis was performed using a Shimadzu RF6000 spectrofluorophotometer (Japan). 280 nm was set as the excitation wavelength, and the results were recorded from 290 to 500 nm.

### 2.11 Protease and thermostability of free and immobilized enzymes

To this aim, a water bath at 52 $^0$C was prepared to incubate the free and immobilized enzyme for 120 min. The residual activity of both L-ASNase was recorded in 30 min intervals. Trypsin was picked for the protease stability evaluation of free and immobilized enzymes. The catalytic activity of free and immobilized enzymes was determined in time periods of 30 to 120 min.

### 2.12 Reusability

After each enzymatic reaction at optimum conditions, the immobilized L-ASNase was collected with a magnet, and the residual activity was measured to indicate the reusability of the enzyme.

### 2.13 Effect of storage on long-term stability

Free and conjugated enzymes were kept in saline buffer (pH 8) at 4 $^0$C for 30 days. The remaining activity of L-ASNase was determined over 4 d intervals under optimum conditions.

## 3. Results and discussion

### 3.1 NPs FTIR analysis

FTIR analysis of the $Fe_3O_4$, $Fe_3O_4$@Au core-shell, $Fe_3O_4$@Au@Cysteine, and L-ASNase binding onto $Fe_3O_4$@Au@Cysteine is shown in Figure 1. Peaks at 560 cm$^{-1}$ and 1630 cm$^{-1}$ are pursuant to Fe-O, and a peak at 1586 cm$^{-1}$ pointing to carboxylic groups of citrate confirmed the formation of $Fe_3O_4$ NPs. The potency of peaks at 560 cm$^{-1}$ and 1586 cm$^{-1}$ was decreased, confirming the formation of a core-shell (Sedki et al., 2021). Modification with cysteine was confirmed by characteristic peaks at 2539 cm$^{-1}$ (attributed to SH stretching) and 2922 cm$^{-1}$ (symmetric stretching vibrations $CH_2$). A peak at 3544 cm$^{-1}$ that is evinced to N-H was observed after the immobilization process by EDC and NHS (Kamali et al., 2021). After enzyme binding on the modified NPs, some new peaks were observed. Peaks at 1636 cm$^{-1}$ and 1544 cm$^{-1}$ are attributed to amide I bending and amide II bending from the polypeptide chain of L-ASNase. Also, peaks at 2900-2972 cm$^{-1}$ and 3200-3600 cm$^{-1}$ are attributed to N-H stretching and aromatic C-H stretching vibrations, respectively (Bahreini et al., 2014).

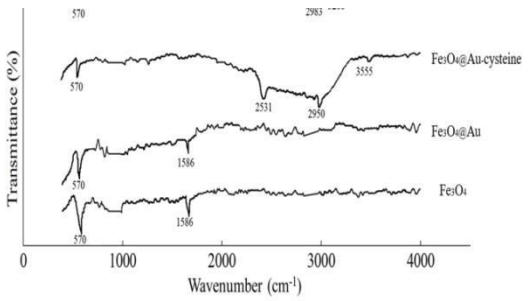


**F**

**igure 1**. FTIR pattern collected for free magnetic, gold capped magnetic, cysteine functionalized gold capped magnetic, and enzyme contains cysteine functionalized gold capped magnetic NPs.

### 3.2 Microscopic analysis of NPs

SEM analysis showed that $Fe_3O_4$ NPs had unique morphology, and after the formation of the Au shell, the diameter of the NPs increased without any change in their morphology (Figure 2 A). The Au layer has high electron density; therefore, the comparison of TEM graphs indicates that $Fe_3O_4$ NPs are brighter than $Fe_3O_4$@Au (Figure 2 B) (Salehizadeh et al., 2012).

### 3.2 Microscopic analysis of NPs

SEM analysis showed that $Fe_3O_4$ NPs had unique morphology, and after the formation of the Au shell, the diameter of the NPs increased without any change in their morphology (Figure 2 A). The Au layer has high electron density; therefore, the comparison of TEM graphs indicates that $Fe_3O_4$ NPs are brighter than $Fe_3O_4$@Au (Figure 2 B) (Salehizadeh et al., 2012).

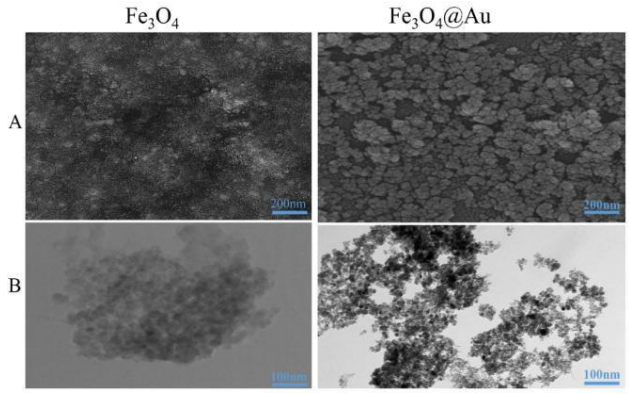


**Figure 2**. The surface analysis of NPs specimens. A) SEM images of free and gold-shell magnetic NPs at a scale of 200 nm; B) TEM images of free and magnetic NPs capped by gold-shell at a scale of 100 nm.

### 3.3 UV-Vis and XRD analysis of NPs

The formation of $Fe_3O_4$ NPs as a core and the surface coverage of the Au shell to create a $Fe_3O_4$@Au core-shell were confirmed using UV-Vis (Figure 3 A). Iron NPs did not show any characteristic adsorption peak, and their adsorption decreased gradually (Kozenkova et al., 2020). After placing the Au shell on the surface of the $Fe_3O_4$ NPs, a peak was created at about 525-537 nm.

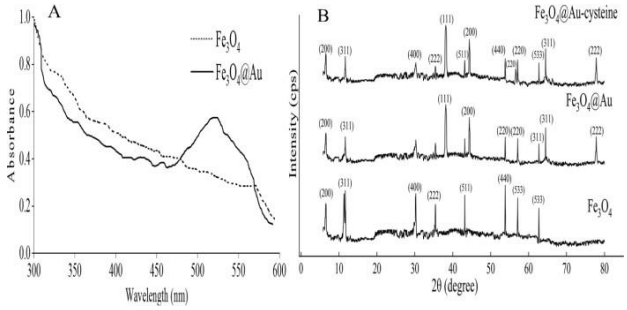


**Figure 3**. A) UV-Vis spectra of fabricated NPs, the absorbance of samples were measured at a wavelength of 300-600 nm. B) XRD spectrum of magnetic, gold-shell magnetic, and cysteinefunctionalized gold-shell NPs.

The results of XRD have been shown in Figure 3 B. Eight characteristic peaks of iron NPs at 2θ values of 75.45, 57.45, 53.54, 44.89, 36.87, 31.67, 12.67 and 7.23 corresponding to (311), (400), (440), (511), (222), (200), and (533) were observed. New peaks at 2θ values 77.78, 63.44, 38.81, and 43.24 corresponding to (222), (311), (111), and (200) are attributed to the Au layer on the surface of $Fe_3O_4$ NPs. The comparison of XRD patterns confirmed that Au and cysteine binding onto the surface of $Fe_3O_4$ NPs decreased the intensity of peaks of iron NPs. These findings are in line with other studies. For instance, a similar study reported no significant change in the XRD pattern of Fe3O4@Au after functionalization with cysteine (Zhang et al., 2021). Figure 4 shows the elemental analysis of $Fe_3O_4$ NPs before and after combination with Au and modification of the core-shell with cysteine and L-ASNase immobilization onto the core-shell using EDX. Carbon, oxygen, and iron peaks confirm the formation of $Fe_3O_4$ NPs. After the formation of the core-shell, an Au peak is observed, and a decrease in the intensity of iron and oxygen peaks has occurred. An increase in the intensity of the carbon peak and the emergence of the sulfur peak is attributed to cysteine. The presence of a nitrogen peak and the increase in the intensity of carbon and sulfur peaks are attributed to amino acids of L-ASNase

immobilized onto the core-shell (Orhan & Aktaş Uygun, 2020).

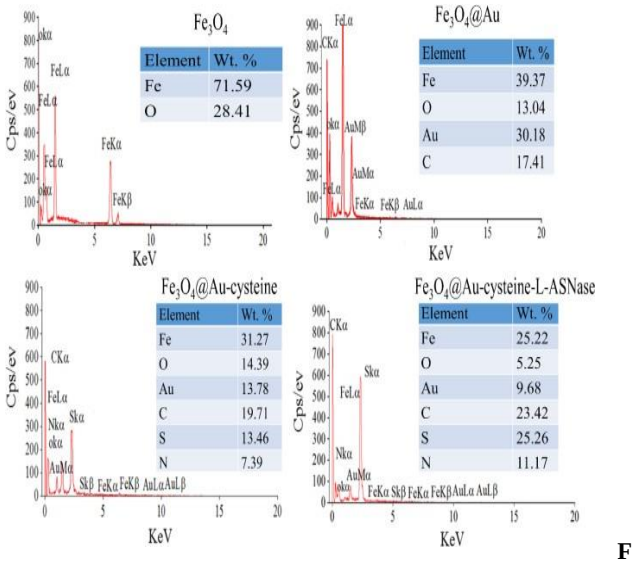


**Figure 4**. Elemental content analysis of NPs.

### 3.4. Analysis of the secondary structure

CD analysis at the Far-UV range showed that the free L-ASNase is composed of 41% of α-helix, 40% β-sheet, and 19% of random-coil (Figure 5). The relative abundance of secondary structures was changed after the immobilization of the enzyme. The abundance of α-helix, β-sheet, and random-coil in immobilized enzymes was 44%, 45%, and 11%, respectively. Adsorption peaks at 208 nm and 222 nm are attributed to α-helix, and peaks at 217-220 nm are attributed to β-sheet. There was a slight change in ellipticity which can be related to lower steric hindrance between enzyme and matrix because of the presence of cysteine (Ashrafi et al., 2013).

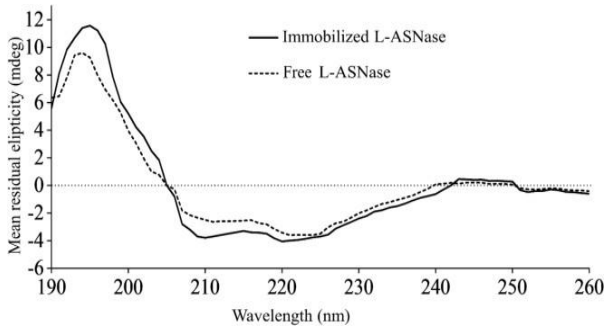


**Figure 5**. Secondary structure analysis of the free and immobilized enzyme.

### 3.5 Analysis of the tertiary structure

The three-dimensional conformation shows a critical performance in the active site function of an enzyme. Therefore, the structural alterations in three-dimensional conformation of L-ASNase were evaluated before and after immobilization using fluorescence spectroscopy and the spectra were recorded at 290-600 nm (Figure 6). L-ASNase has tryptophan in each sub-unit. So, the highest fluorescence emission of both free and conjugated enzyme was observed at 340 nm (Chahardahcherik et al., 2020). The decrease in fluorescence emission of the immobilized enzyme can be related to alteration in the environment of tryptophan amino acids. In addition, the similarity between emission patterns of free and immobilized enzymes can be concluded that the change in the tertiary structure of the immobilized enzyme was not significant (Possarle et al., 2020).

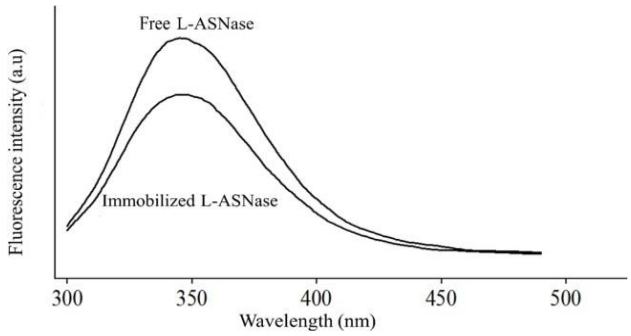


**Figure 6**. Analysis of the tertiary structure of the free and immobilized enzyme.

### 3.6 Kinetics of free and immobilized L-ASNase

The results showed that the Km value decreased from 4.43±0.05 to 3.75±0.12 mM after immobilization (Figure 7). Also, the Vmax parameter for the immobilized enzyme increased from 187.23±11 to 224.78±16 μM min-1mg-1 compared to the free enzyme. These results showed that the affinity of the immobilized enzyme for L-ASNase was increased (Ates et al., 2018). Furthermore, the interactions between substrate and enzyme result in increased Vmax,

possibly due to the appropriate conformation of the immobilized enzyme and an increase in the substrate delivery to the active site (Noma et al., 2021). These observations confirmed that the alterations in the secondary and tertiary structure of L-ASNase were not remarkable.

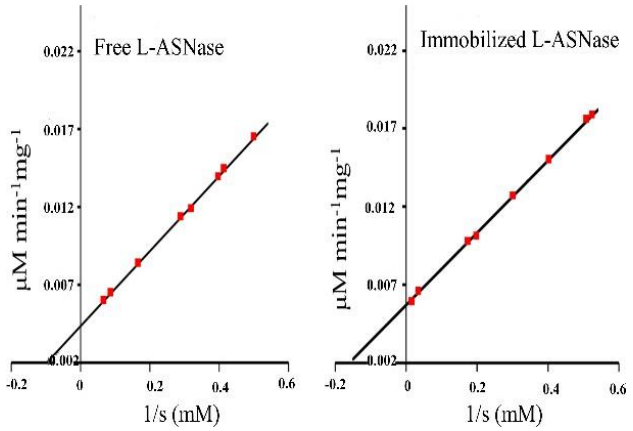


**Figure 7**. Calculation of km and Vmax by Michalis-Menten linear plot of A) the free enzyme and B) the immobilized enzyme.

### 3.7 Conjugation efficiency of core-shell NPs

Immobilization of the enzyme on a $Fe_3O_4$@Au core-shell functionalized by cysteine was carried out by EDC/NHS reagent. The efficiency of $Fe_3O_4$@Au-cysteine was determined at 83.27%.

### 3.8 Optimum pH and temperature

The analysis of the catalytic activity of free and immobilized enzymes under different pH values showed that the conjugated enzyme was more active under alkaline conditions, and the maximum activity was achieved at pH 5.5. The highest activity of the free enzyme was achieved at pH 8.1. Presumably, immobilization of L-ASNase by cysteine cross-linkers caused appropriate orientation of the enzyme active site and improved the affinity between the substrate and the active site of the enzyme. In addition, the activity of the conjugated L-ASNase at higher temperatures was more than the free enzyme. The L-ASNase's strong binding to the NP's surface protected the enzyme structure and active site of the enzyme against thermal variations (Figure 8).

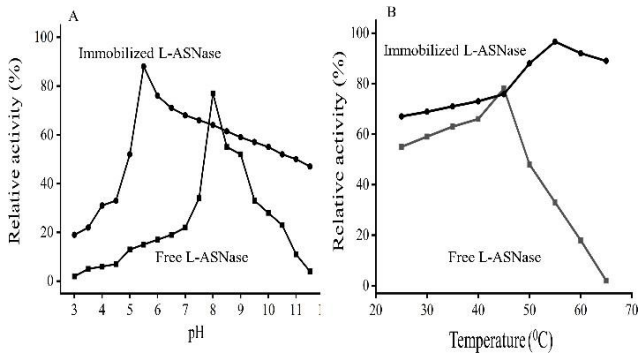


**Figure 8**. Free and immobilized enzyme catalytic activity. A) Relative activity at several pH values and B) Relative activity at several temperatures.

### 3.9 Free and immobilized L-ASNase resistance features examination

The analysis of the resistance of the immobilized enzyme against trypsin (as a model protease) suggested that after 120 min incubation, the conjugated enzyme held about 86% of its activity. However, the function of the free enzyme after 120 min incubation with trypsin was less than 37% (Figure 9 A). Also, the reusability analysis showed that after 15 cycles of the enzymatic reaction, the conjugated enzyme kept about 72% of its activity (Figure 9 B).

The effect of storage was distinguished between free and immobilized L-ASNase by maintaining them at 25 ◦C for a five-day period (Figure 9 C). After immobilization, the long-time resistance of the immobilized enzyme was augmented compared to compared to the free L-ASNase. At the end of 30 days, the conjugated enzyme showed more than 88 % of its activity, while the free enzyme activity fell to less than 40%.

To study the effect of temperature on the free and immobilized enzymes, their activity was examined each 30 min at 52 °C, and the outcomes are indicated in Figure 9 D. After 1 h incubation at 52 °C, the remaining activity of the free enzyme was reduced step by step so that after 3 h the free enzyme lost a large percentage of its activity. However, the rate of activity loss was very low for the immobilized enzyme. In the same conditions, the remaining activity of the free enzyme was less than 45%, but the conjugated enzyme maintained more than 86% of

its activity. These findings are in agreement with previous reports. For example, Verma et al. (2013) showed that the immobilization of β-glucosidase onto magnetic NPs enhanced the thermostability of this enzyme compared to the free one.

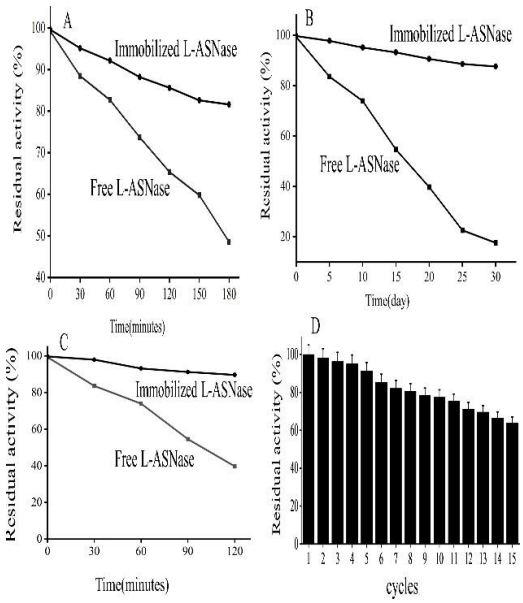


**Figure 9.** Resistance characterization of samples. A) comparison between free and immobilized enzymes toward protease reaction. B) Enumeration of reusable cycles for the enzymes after immobilization. C) Effect of immobilization process on the long-term stability of the enzymes, residual activity reported at intervals of 30 days. D) Enzyme thermostability, both enzymes were incubated for 180 min at 52 ˚C, and their residual activity was reported.

## 4. Conclusion

Fe3O4@Au NPs are considered appropriate matrices due to the presence of various matrices, exposed magnetic properties, significant biocompatibility, and excellent physical and chemical stability. Fe3O4@Au NPs containing short-chained cross-linkers show better efficiency due to increased NPs surfaces, agglomeration and denaturation prevention, and lack of matrix-enzyme steric hindrance. L-ASNase is known as an important anticancer therapeutic agent. Therefore, in recent years, much research has been conducted to improve its catalytic and biochemical features and its stability under different physiologic conditions. In the current study, the immobilization technique using magnetic NPs was employed to achieve this end. Magnetic Fe3O4@Au@cysteine core-shell NPs were fabricated and characterized using XRD, TEM, SEM, FTIR and EDX analysis. According to the results of this study, the immobilized L-ASNase tendency to its substrate and its stability and reusability was increased significantly compared to the free enzyme. Also, the secondary and tertiary structures of the immobilized enzymes rarely changed. Therefore, it can be concluded that the conjugation of L-ASNase on magnetic iron NPs is an efficient method to amplify the biochemical properties of this enzyme. Finally, it is suggested that, i) Other L-ASNase enzyme sources can be used for the immobilization process. ii) Other nano-carriers can be used as a matrix, like silver, platinum NPs, quantum dots and other supports. iii) Simultaneous immobilization of anticancer drugs like glutaminase, paclitaxel and other drugs be investigated to improve their anticancer characteristics.

## Conflict of interest

The contents of the manuscript approved by all co-authors, and there is no conflict of interest to report.

## Ethical approval

For this article, human and animal experiments are not considered.

## Acknowledgments

All authors would like to thank, the Science and Research Branch, Islamic Azad University of Tehran, laboratory of Bioanalysis in IBB of University of Tehran, and Department of Microbial Biotechnology in University of Tehran.

## Open access

## References


Agrawal, S., & Kango, N. (2019). Development and catalytic characterization of L-ASNase nano- bioconjugates. International journal of biological macromolecules, 135, 1142-1150. doi: 10.1016/j.ijbiomac.2019.05.154

Ashrafi, H., Amini, M., Mohammadi-Samani, S., Ghasemi, Y., Azadi, A., Tabandeh, M. R., ... & Daneshamouz, S. (2013). Nanostructure L-ASNase-fatty acid bioconjugate: synthesis, preformulation study and biological assessment. International journal of biological macromolecules, 62, 180-187.
doi: 10.1016/j.ijbiomac.2013.08.028

Ates, B., Ulu, A., Köytepe, S., Noma, S. A. A., Kolat,

V. S., & Izgi, T. (2018). Magnetic-propelled Fe 3 O 4–chitosan carriers enhance L-ASNase catalytic activity: a promising strategy for enzyme immobilization. RSC advances, 8(63), 36063-36075. doi: 10.1039/C8RA06346J

Bahreini, E., Aghaiypour, K., Abbasalipourkabir, R., Mokarram, A. R., Goodarzi, M. T., & Saidijam, M. (2014). Preparation and nanoencapsulation of L-ASNase II in chitosan-tripolyphosphate nanoparticles and in vitro release study. Nanoscale research letters, 9(1), 1-13. doi: 10.1186/1556-276X-9-340

Bilal, M., Zhao, Y., Rasheed, T., & Iqbal, H. M. (2018). Magnetic nanoparticles as versatile carriers for enzymes immobilization: A review. International journal of biological macromolecules, 120, 2530-2544. doi: 10.1016/j.ijbiomac.2018.09.025

Bilal, M., Zhao, Y., Rasheed, T., & Iqbal, H. M. (2018). Magnetic nanoparticles as versatile carriers for enzymes immobilization: A review. International journal of biological macromolecules, 120, 2530-2544. doi: 10.1016/j.ijbiomac.2018.09.025

Chahardahcherik, M., Ashrafi, M., Ghasemi, Y., & Aminlari, M. (2020). Effect of chemical modification with carboxymethyl dextran on kinetic and structural properties of L-ASNase. Analytical biochemistry, 591, 113537. doi: 10.1016/j.ab.2019.113537

Datta, S., Christena, L. R., & Rajaram, Y. R. S. (2013). Enzyme immobilization: an overview on techniques and support materials. 3 Biotech, 3(1), 1-9. doi: 10.1007/s13205-012-0071-7

Dong, H., Li, J., Li, Y., Hu, L., & Luo, D. (2012).

Improvement of catalytic activity and stability of lipase by immobilization on organobentonite. Chemical Engineering Journal, 181, 590-596. doi: 10.1016/j.cej.2011.11.095

Federsel, H. J., Moody, T. S., & Taylor, S. J. (2021). Recent trends in enzyme immobilization—concepts for expanding the biocatalysis toolbox. Molecules, 26(9), 2822. doi:10.3390/molecules26092822

Hariani, P. L., Faizal, M., Ridwan, R., Marsi, M., & Setiabudidaya, D. (2013). Synthesis and properties of $Fe_3O_4$ nanoparticles by co-precipitation method to removal procion dye. International Journal of Environmental Scienceand Development, 4(3), 336-340.
doi:0.7763/IJESD. 2013.V4.366

Kamali, P., Zandi, M., Ghasemzadeh-Moghaddam, H., & Fani, M. (2022). Comparison between various biosensor methods for human T-lymphotropic virus-1 (HTLV-1) detection. Molecular Biology Reports, 49(2), 1513-1517. doi: 10.1007/s11033-021-06959-w

Kozenkova, E., Levada, K., Efremova, M. V., Omelyanchik, A., Nalench, Y. A., Garanina, A. S., ... & Rodionova, V. (2020). Multifunctional Fe3O4-Au nanoparticles for the MRI diagnosis and potential treatment of liver cancer. Nanomaterials, 10(9), 1646. doi: 10.3390/nano10091646

Lee, C. H., Jin, E. S., Lee, J. H., & Hwang, E. T.(2020). Immobilization and stabilization of enzyme in biomineralized calcium carbonate microspheres. Frontiers in Bioengineering and Biotechnology, 8, 553591. doi: 10.3389/fbioe.2020.553591

León Félix, L., Coaquira, J. A. H., Martínez, M. A. R.,Goya, G. F., Mantilla, J., Sousa, M. H., ... & Morais, P. C. (2017). Structural and magnetic properties of core-shell Au/Fe3O4 nanoparticles. Scientific reports, 7(1), 1-8. doi: 10.1038/srep41732

Narayana, K. J. P., Kumar, K. G., & Vijayalakshmi,M. (2008). L-ASNase production by Streptomyces albidoflavus. Indian Journal of Microbiology, 48(3), 331-336. doi: 10.1007/s12088-008-0018-1Noma, S. A. A., Yılmaz, B. S., Ulu, A., Özdemir, N., & Ateş, B. (2021). Development of L-ASNase@ hybrid nanoflowers (L-ASNase@ HNFs) reactor system with enhanced enzymatic reusability and stability. Catalysis Letters, 151(4), 1191-1201. doi: 10.1007/s10562-020-03362-1

Orhan, H., & Aktaş Uygun, D. (2020). Immobilization of L-ASNase on magnetic nanoparticles for cancer treatment. Applied biochemistry and biotechnology, 191(4), 1432-1443. doi: 10.1007/s12010-020-03276-z

Possarle, L. H. R. R., Junior, J. R. S., & Caseli, L. (2020). Insertion of carbon nanotubes in Langmuir-Blodgett films of stearic acid and L-ASNase enhancing the catalytic performance. Colloids and Surfaces B: Biointerfaces, 192, 111032. doi: 10.1016/j.colsurfb.2020.111032

Salehizadeh, H., Hekmatian, E., Sadeghi, M., & Kennedy, K. (2012). Synthesis and characterization of core- shell Fe3O4-gold-chitosan nanostructure. Journal of nanobiotechnology, 10(1), 1-7.Doi:10.1186/1477-3155-10-3

Salihov, S. V., Ivanenkov, Y. A., Krechetov, S. P., Veselov, M. S., Sviridenkova, N. V., Savchenko, A. G., & Majouga, A. G. (2015). Recent advances in the synthesis of $Fe_3O_4$@ AU core/shell nanoparticles. Journal of magnetism and magnetic materials, 394, 173-178. doi: 10.1016/j.jmmm.2015.06.012

Sedki, M., Zhao, G., Ma, S., Jassby, D., & Mulchandani, A. (2021). Linker-Free Magnetite-Decorated Gold Nanoparticles (Fe3O4-Au): Synthesis, Characterization, and Application for Electrochemical Detection of Arsenic (III). Sensors, 21(3), 883. doi: 10.3390/s21030883

Soares, A. L., Guimaraes, G. M., Polakiewicz, B., de Moraes Pitombo, R. N., & Abrahão-Neto, J. (2002). Effects of polyethylene glycol attachment on physicochemical and biological stability of E. coli L-ASNase. International journal of pharmaceutics, 237(1-2), 163-170. doi: 10.1016/S0378-5173(02)00046-7

Sohrabi, N., Rasouli, N., & Torkzadeh, M. (2014). Enhanced stability and catalytic activity of immobilized α- amylase on modified $Fe_3O_4$ nanoparticles. Chemical EngineeringJournal, 240, 426-433. doi: 10.1016/j.cej.2013.11.059

Tamer, U., Gündoğdu, Y., Boyacı, İ. H., & Pekmez, K. (2010). Synthesis of magnetic core–shell Fe3O4–Au nanoparticle for biomolecule immobilization and detection. Journal of Nanoparticle Research, 12(4), 1187- 1196. dio: 10.1007/s11051-009-9749-0

Verma, M. L., Chaudhary, R., Tsuzuki, T., Barrow, C. J., & Puri, M. (2013). Immobilization of β-glucosidase on a magnetic nanoparticle improves thermostability: application in cellobiose hydrolysis. Bioresource technology, 135, 2-6. doi: 10.1016/j.biortech.2013.01.047

Wriston, J. C., & Yellin, T. O. (1973). L-ASNase: a review. Adv Enzymol Relat Areas Mol Biol, 39, 185-248. doi: 10.1002/9780470122846.ch3.

Yazdani, F., & Seddigh, M. (2016). Magnetite nanoparticles synthesized by co-precipitation method: The effects of various iron anions on specifications. Materials Chemistry and Physics, 184, 318-323. doi: 10.1016/j.matchemphys.2016.09.058

Zhang, T., Lei, L., Tian, M., Ren, J., Lu, Z., Liu, Y., & Liu, Y. (2021). Multifunctional Fe3O4@ Au supraparticle as a promising thermal contrast for an ultrasensitive lateral flow immunoassay. Talanta, 222, 121478. doi:10.1016/j.talanta.2020.121478